Optics & Laser Technology 171 (2024) 110458

Contents lists available at ScienceDirect

Optics and Laser Technology

journal homepage: www.elsevier.com/locate/optlastec

Full length article

Simulation of spatial rogue waves in actively Q-switched solid-state laser with transverse mode locking

Roza Navitskaya [a,b,*], Ihar Stashkevich [a], Stanislav Derevyanko [b], Alina Karabchevsky [b,**]

[a] Faculty of Physics, Belarusian State University, 4 Nezalezhnasti Avenue, Minsk, 220030, Belarus

[b] School of Electrical and Computer Engineering, Ben-Gurion University of the Negev, Beer-Sheva, 8410501, Israel

ARTICLE INFO

Keywords:
Spatial rogue waves
Transverse mode locking
Multi-mode laser
Active Q-switching

ABSTRACT

We report the generation of spatial rogue waves in the actively Q-switched Nd:YAG laser with several transverse modes and negligible nonlinear effects in the cavity. We discuss a basic theoretical model that is able to reproduce the experimental observations of spatial rogue waves in the output Q-switched pulses as a result of the coherent superposition of transverse modes. The simulated rogue wave statistics depends on the configuration of the lasing modes and take a more pronounced L-shaped form in the case of highly anisotropic mode distribution and reduced frequency spacing between the modes. For larger frequency spacing between the modes, the mode-locking effects result in the periodic dynamics of the transverse beam profile and formation of spatio-temporal rogue waves. These results indicate that transverse mode-locking and spatial symmetry breaking through anisotropy in the mode configuration represent factors responsible for spatial rogue wave emergence in multimode lasers with low nonlinearity.

1. Introduction

Recently, the phenomenon of rogue waves (RWs) has been the focus of interest in different fields of optics. After the first observation of optical RWs through supercontinuum generation in a highly nonlinear fiber [1], they were investigated in various optical systems. Laser dissipative systems provide well-developed platforms for the study of RWs [2,3]. Depending on the laser system properties, such types of rogue waves as temporal, spatial, or spatio-temporal can be observed, which represent optical pulses with extremely high amplitudes tightly focused in the corresponding dimensions. It is known that the rogue wave emergence in lasers is mainly governed by the interplay of gain, dispersion, and nonlinearity, and can be assisted by spatial effects as well [2,4,5]. However, the exact role of nonlinearity and spatial effects in the process of spatial and spatio-temporal RWs formation in lasers is still under investigation. The study of spatial and spatio-temporal RWs, apart from being interesting from a physical point of view, has also an important practical aspect as such kind of events are the most unpredictable and dangerous ones - in the case of high powers they may easily lead to the onset of the nonlinear effect of catastrophic self-focusing and result in the damage of laser elements, which was observed in real laser systems [6].

There are different types of nonlinear properties that could be present in laser systems, including self-focusing, saturable absorption, thermal nonlinearity, and nonlinear gain competition. Usually, high self-focusing or saturable absorption nonlinearity is a sufficient factor for spatial RWs generation in lasers, e.g. due to the effects of filamentation in an amplified Kerr media [7], multiple soliton formation in fiber lasers with spatiotemporal mode-locking [8,9], and nonlinear chaotic dynamics of semiconductor lasers with intracavity saturable absorbers [10,11]. Also, the formation of spatio-temporal extreme events was observed in high-power solid-state lasers due to the spontaneous synchronization of laser modes assisted by self-focusing in the active medium [6].

Nevertheless, there are examples of spatial RWs generation in purely linear optical systems [4,12–15], indicating that high nonlinearity is not always necessary for their formation. Typically, such systems possess several common properties. One of them is a large number of interacting transverse modes, which makes it possible to obtain diverse configurations in the spatial domain. Another one is the presence of some factor that causes correlations or inhomogeneity in the distribution of the interacting waves characteristics. This could be, for example, an inaccessible range of values in the phase probability distribution [12], an inhomogeneous mask in the spatial domain [13], the

* Corresponding author at: Faculty of Physics, Belarusian State University, 4 Nezalezhnasti Avenue, Minsk, 220030, Belarus.
** Corresponding author.
E-mail addresses: r.navitskaya@gmail.com (R. Navitskaya), alinak@bgu.ac.il (A. Karabchevsky).

https://doi.org/10.1016/j.optlastec.2023.110458
Received 12 October 2023; Received in revised form 19 November 2023; Accepted 8 December 2023
Available online 15 December 2023

presence of strong focusing regions in random medium [15], or long-range correlations between the phases of interfering waves [14]. The interplay of these two properties can lead to the outstanding L-shaped statistics characteristic of the observed rogue waves. In a similar way, linear propagation effects could assist the onset of RWs in nonlinear systems, which are further enhanced by nonlinearity [4].

In dissipative laser systems, the generation of spatial RWs under low nonlinearity was experimentally observed in actively Q-switched Nd:YAG laser operating at multiple transverse mode regime [16]. In these experiments, the strength of self-focusing and thermal nonlinearity was reduced to a negligible level by using relatively small pump powers. To obtain spatial RWs in the output beam, laser generation at multiple high-order transverse modes was required, which was achieved by adjusting the configuration of the laser cavity. However, several questions still remained open. First, it was not possible to completely eliminate nonlinearity as nonlinear gain competition is an intrinsic property of a laser system. Second, the emergence of RWs was a random effect observed for some positions of the laser mirrors obtained using manual adjustment and disappeared for different mirror configurations even if all other parameters were kept unchanged. Therefore, it is not completely clear whether the laser nonlinearity still plays an important role and exactly which cavity parameters are crucial for spatial rogue wave emergence.

One of the possible mechanisms that could be responsible for the onset of spatial and spatio-temporal RWs in multi-mode lasers under low nonlinearity is the spontaneous synchronization of transverse laser modes or both transverse and longitudinal modes.

Transverse mode-locking in lasers is a well-known effect, which was investigated theoretically in early works [17–19]. By analogy with the longitudinal mode locking, the synchronization of transverse modes results in a confined field pattern that moves in the transverse plane of the beam at a frequency defined by the frequency spacing between the locked modes [17]. The transverse mode locking of high-order Hermite-Gaussian modes was experimentally demonstrated in an end-pumped solid-state laser, which resulted in a periodically scanning output beam with the time-dependent spot size [20].

Besides, the synchronization of both longitudinal and transverse modes was also investigated. This can be realized either as independent synchronization of axial modes for each of the transverse modes, so that there are several independent mode-locked pulses propagating in the cavity, or as total mode-locking corresponding to a single confined pulse [18]. In the latter case, for certain relations between the transverse mode frequency spacing and the cavity round-trip time, the mode-locked pulse can propagate along a closed trajectory in the cavity, which results in a multi-periodic behavior of the laser. Total mode locking of such kind was observed experimentally in different types of lasers, including He–Ne laser [21], CO_2 laser [22], Nd^{3+} glass laser [23], Yb:CaF_2 bulk laser [24], and Ti:Sapphire laser operating at several transverse modes, which corresponded to period doubling, tripling and quadrupling for certain cavity configurations [25–27]. In addition, the interaction of multiple transverse modes in the passively mode-locked solid-state laser can lead to amplitude instability in the output pulse train and break-up of the continuous-wave mode-locking [28]. Transverse mode-locking was demonstrated also in microcavity lasers [29], VCSELs [30,31], and ultracompact semiconductor lasers [32]. Besides, the physics of spatio-temporal mode-locking was intensively investigated in multi-mode fiber lasers, indicating the importance of modal interactions and mode-dependent effects in the complex laser dynamics [8,9,33,34]. It was shown that transverse mode configuration affects the spatio-temporal build-up dynamics, resulting in different modal content of multiple dissipative solitons [34].

In large aperture lasers operating in the multi-mode regime, e.g. lasers with relatively high Fresnel number, spatially complex output beam patterns were observed as a result of the coupled dynamics of many modes. Usually, the dynamics in such lasers is investigated in terms of time-averaged patterns. In such case, the presence of transverse mode-locking can be indicated by symmetry breaking in the averaged patterns [35], which means that a coherent superposition of the laser modes takes place. Besides, it was experimentally observed that broad-area lasers can exhibit fast spatial dynamics. For example, in CO_2 laser dynamically changing patterns including bright filaments were observed, which were different from the regular time-averaged intensity patterns [36]. In such patterns, the filaments were randomly distributed and had lifetimes of about 2 ns. A dynamic transition of laser patterns from a boundary-controlled to a turbulent-like regime was experimentally observed in a broad-area Nd:YAG laser with Fresnel number about 50 [37]. Depending on the pump power, which determined the strength of the laser nonlinearity, the time required for such a transition was about tens of μs or less.

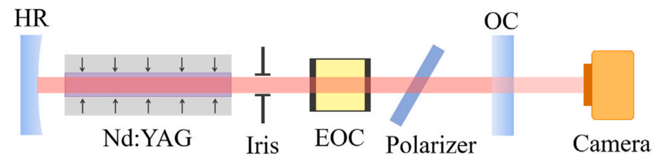

Fig. 1. Schematic of the actively Q-switched laser considered in the simulation. HR: highly-reflective concave mirror, Nd:YAG: laser active element with flashlamp pumping, EOC: electro-optic shutter, OC: flat output mirror.

Thus, multiple experimental observations and theoretical studies indicate that different types of multi-mode lasers can exhibit outstanding spatio-temporal dynamics, which is especially pronounced in broad-area lasers supporting a large number of transverse modes. In such kinds of lasers operating in specific multi-mode regimes, there is a tendency for hot spots formation that could transform into spatial rogue waves under certain conditions favorable for spontaneous mode-locking.

Aided by this knowledge, in this paper we investigate the possibility of spatial RWs generation as a result of spontaneous transverse mode locking in a multi-mode solid-state laser. We consider an actively Q-switched Nd:YAG laser with a setup described in our previous experiments [16], where the observed transverse beam profiles were measured by a camera and corresponded to averaged beam patterns integrated over the entire Q-switched pulse length.

We explore a simple theoretical model based on the laser rate equations that could be used to calculate the output laser beam profile in a setup shown in Fig. 1 mimicking the experimental conditions [16]. We investigate the rogue wave statistics depending on the laser mode configuration and frequency separation between the transverse modes, which is considered a free parameter depending on the cavity configuration (e.g. positions of the mirrors).

2. Theory

To simulate the generation of spatial RWs and investigate their properties, the temporal and spatial dynamics of the output laser beam need to be calculated. Advanced simulations of spatio-temporal effects and dynamics of the transverse beam profile in lasers can be performed using the Maxwell–Bloch equations [35–39]. This model is relevant for the case of class-B multi-mode lasers, such as some solid-state ones, where the dynamics of the population inversion need to be considered as its decay rate is comparable to the optical field relaxation rate [38]. In the case of class-A lasers, when polarization and population inversion decay significantly faster than the optical field, the Maxwell–Bloch equations can be reduced to the complex Ginzburg–Landau equation, which is typically used for the fiber laser modeling [38,40].

Although the Maxwell–Bloch model provides an advanced means for simulation and analysis of the laser transverse dynamics, it is quite complex and computationally expensive. This could make it difficult to adjust the model parameters to reproduce the behavior of a realistic laser system. In addition, the analysis of rogue wave statistics and properties requires thousands of simulation iterations to obtain data for different laser system parameters and initial conditions, which would take a great deal of time using such a complex model. Therefore, a more simple model would be desirable that could be used to describe the spatial rogue waves emergence in laser systems.

One of the approaches to perform the simplified analysis is based on the direct superposition of the laser transverse modes, e.g. from a set of Hermite-Gaussian (HG) or Laguerre-Gaussian (LG) modes with different amplitudes and phases [29]. Usually, the transverse modes of the laser cavity are well described by HG modes for rectangular geometry or LG modes for circular geometry [41].

In general, the operation regime of a multi-mode laser depends on the number of supported transverse modes and the frequency separation between them [35,37]. The number of transverse modes that can oscillate in the laser cavity can be estimated by the Fresnel number, which is the ratio between the cavity aperture area and the fundamental mode area [35] $F = (b/2)^2/(\lambda L)$. Here b is the transverse size of the aperture in the cavity, L is the cavity optical length and λ is the wavelength. The Fresnel number determines the maximal index of the supported transverse mode.

The frequency of a longitudinal mode q corresponding to a transverse TEM_{mn} mode is given by [41,42]

$$\nu_{qmn} = [q + q' \arccos(\sqrt{g_1 g_2})/\pi]\frac{c}{2L} \tag{1}$$

where g_1, g_2 stand for the cavity parameters and q' is the total transverse modal number that depends on the symmetry of the problem. It is equal to $q' = m+n+1$ for HG modes and $q' = 2m+n+1$ for LG modes, where m and n define two transverse mode numbers for HG modes or radial and azimuthal modal indices for LG modes.

Regardless of the symmetry, for the plano-concave cavity configuration $g_1 = 1$ and $g_2 = 1 - L/R$, so the frequency separation between transverse modes is given by

$$\Delta\nu_t = \frac{c}{2\pi L}\arccos(\sqrt{1 - L/R}) \tag{2}$$

where R is the radius of the concave mirror.

Usually, the superposition of transverse modes is considered within the same degenerate family (equal values of q') as this corresponds to stationary beam patterns, which cannot be obtained by coupling of transverse modes from different families due to different optical frequencies of the modes [29]. However here we will consider a different case, namely a coherent superposition of different transverse modes to analyze dynamically changing output beam patterns that may contain spatial or spatio-temporal rogue waves.

Thus, the total near-field amplitude and intensity distributions can be represented through a sum of modal fields with slowly varying amplitudes A_{qmn}, frequencies ν_{qmn}, and phases ϕ_{qmn} [20]:

$$E(x, y, z, t) = \sum_{q,m,n} A_{qmn}(t)U_{mn}(x, y, z)e^{2\pi i\nu_{qmn}t + i\phi_{qmn}} \tag{3}$$

$$I(x, y, z, t) = |E(x, y, z, t)|^2 \tag{4}$$

Here, the transverse field distributions $U_{mn}(x, y, z)$ can correspond to any given set of laser modes, HG or LG. For a laser operating in the Q-switched regime, the functions $A_{qmn}(t)$ correspond to the amplitudes of the Q-switched pulses for different lasing modes.

The time-averaged intensity distribution is given by:

$$I_{average}(x, y, z) = \frac{1}{T_{exp}}\int_0^{T_{exp}} I(x, y, z, t)dt \tag{5}$$

where T_{exp} was chosen to be larger than the Q-switched pulse duration to match the experimental conditions [16], where a camera captured the average intensity profile of the beam integrated over the entire Q-switched pulse length. The values of T_{exp} used in the simulation were about 0.25-1 μs depending on the input parameters.

The mode-dependent amplitudes can be calculated using the rate equations (6) written for the case of a 4-level solid-state laser [42]:

$$\begin{aligned}
\frac{dS_{qmn}}{dt} &= \frac{S_{qmn}}{T_c}\left[l\sigma_e(N_2 - N_1) - 0.5\ln(1/\rho) - \gamma_{qmn} - \gamma_{EOC}(t)\right]\\
\frac{dN_1}{dt} &= \sigma_e \sum_{q,m,n} S_{qmn}(N_2 - N_1) - \frac{N_1}{\tau_1} + \frac{N_2}{\tau_2}\\
\frac{dN_2}{dt} &= \sigma_e \sum_{q,m,n} S_{qmn}(N_1 - N_2) - \frac{N_2}{\tau_2} + \frac{N_3}{\tau_3}\\
\frac{dN_3}{dt} &= \sigma_a S_{pump}(N_t - N_1 - N_2 - N_3) - \frac{N_3}{\tau_3}
\end{aligned} \tag{6}$$

Here N_1, N_2, N_3 and S_{qmn} stand for the carrier densities and mode-dependent photon flux densities in the cavity averaged over the cavity single-trip time $T_c = L/c$, l is the active medium pump length equal to the laser crystal length, N_t is the total density of Nd^{3+} ions, τ_i define lifetimes at the active medium energy levels, σ_a and σ_e stand for the absorption and emission cross-sections, ρ is the output mirror reflection coefficient, γ_{qmn} characterize the mode-dependent losses in the cavity, and γ_{EOC} stands for the time-dependent losses introduced by the electro-optic crystal that is used to perform active Q-switching. It is described by a step-function, where T_{EOC} defines the moment of time when the active shutter switches off:

$$\gamma_{EOC}(t) = \begin{cases} 1, t < T_{EOC} \\ 0, t \geq T_{EOC}. \end{cases} \tag{7}$$

The quantity S_{pump} is the pump photon flux density that is considered equal for all transverse modes (assuming uniform pumping over the crystal surface and in time). It is calculated as

$$S_{pump} = \frac{P_{pump}}{s_{pump}h\nu_a} = \frac{\eta E_{pump}/T_{pump}}{\pi d l_{pump} h\nu_a} \tag{8}$$

where $P_{pump} = \eta E_{pump}/T_{pump}$ is the pump power defined through the pump energy E_{pump}, duration of the pump pulse T_{pump}, and the radiation absorption efficiency η, $s_{pump} = \pi d l_{pump}$ is the radiated area of the crystal with the diameter d, and $h\nu_a$ is the energy of the absorbed photon.

Finally the mode-dependent amplitudes of the output Q-switched pulses are calculated through the photon flux densities in the cavity as

$$A_{qmn}(t) = \sqrt{k_{out}S_{qmn}(t)h\nu_e} \tag{9}$$

where $k_{out} = 0.5\ln(1/\rho)$ is the fraction of photons emitted through the output mirror, and $h\nu_e$ is the energy of the emitted photon.

The Eqs. (6)–(9) represent the simplest model for the analysis of a Q-switched solid-state laser generation at multiple transverse modes. The rate equations (6) are derived assuming averaged effects of all components in the cavity over the round trip time. The modal interactions in the active medium are not considered, so we are neglecting the effects of nonlinear gain competition in the simulation. The only parameters that could lead to the mode-dependent profiles of the output Q-switched pulses in our model are mode-dependent losses γ_{qmn} and initial photon flux densities $S_{qmn}(t = 0)$.

Using the model described above, we investigate the possibility of spatial rogue waves generation due to the spontaneous transverse mode-locking in the actively Q-switched Nd:YAG laser. The laser parameters used in the model are based on the prototype laser setup involved in the experiments [16] and are described in Table 1. A schematic of the laser setup is shown in Fig. 1.

The mode-dependent profiles of Q-switched pulses were calculated using Eqs. (6)–(9) for the laser parameters summarized in Table 1. To reproduce the average temporal profile of output Q-switched pulses observed in the experiments (specifically, its full width at half maximum), we adjusted the radiation absorption efficiency η. For minimal pump energy of 7 J that was required to obtain spatial rogue waves generation in the experiments [16], the observed FWHM was about 55 ns, which corresponded to $\eta = 1.7\%$ in the simulations. In the considered theoretical model the nonlinear mode competition effects are neglected, so

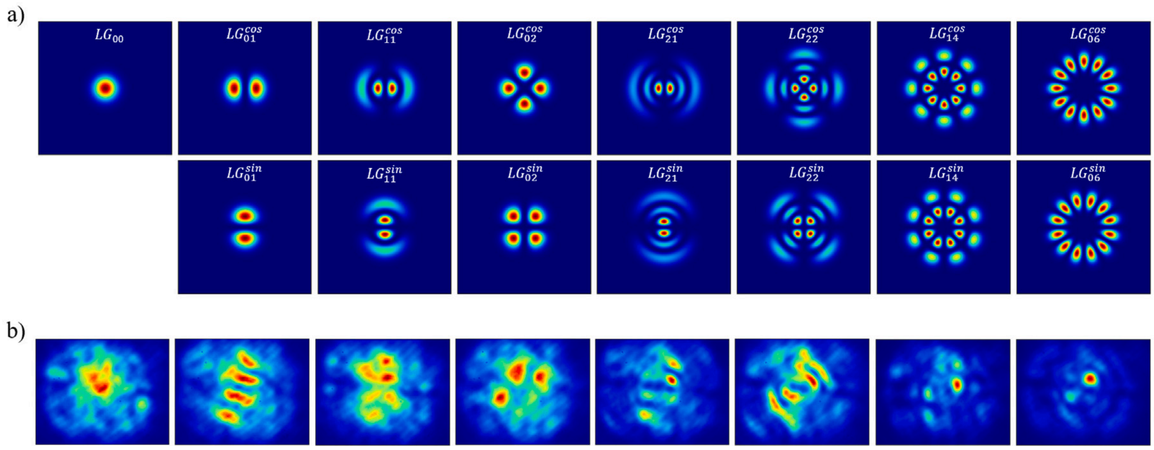

Fig. 2. (a) Lasing modes considered in the simulation; (b) output beam patterns observed in the experiments [16].

Table 1
Nd:YAG laser parameters used in the simulations.

Parameter		Value
Cavity optical length	L	0.782 m
Curvature of the concave mirror	R	3.6 m
Output mirror reflection coefficient	ρ	0.63
Pump energy	E_{pump}	7 J
Duration of the pump pulse	T_{pump}	300 μs
Active shutter switching time	T_{EOC}	150 μs
Nd:YAG crystal length	l	10 cm
Nd:YAG crystal diameter	d	0.5 cm
Pump wavelength	λ_a	808 nm
Generation wavelength	λ_e	1064 nm
Absorption cross-section	σ_a	$7.7 \cdot 10^{-20}$ cm^2
Emission cross-section	σ_e	$28 \cdot 10^{-20}$ cm^2
Total density of Nd^{3+} ions	N_t	$1.38 \cdot 10^{20}$ cm^{-3}
Lifetime at $^4F_{5/2}$ level	τ_3	10 ns
Lifetime at $^4F_{3/2}$ level	τ_2	230 μs
Lifetime at $^4I_{11/2}$ level	τ_1	30 ns

the average power of the output Q-switched pulses has no effect on the beam intensity distribution as long as the normalized intensity statistics is considered. Therefore, this parameter was not taken into account in comparison of the experimental results and simulations. Besides, variations of the peak power of the output Q-switched pulses relative to the average were neglected as well, since their values observed in the experiments were not significant (less than 10%).

For simplicity, we assumed a single longitudinal mode and set the longitudinal mode order q to 0 for all transverse modes. Thus, we limited the analysis to spontaneous synchronization of transverse modes only, while simultaneous locking of both longitudinal and transverse modes is left for future studies.

In the experiments in [16], the number and order of modes was controlled by a circular iris diaphragm, so that the Laguerre-Gaussian mode basis appears to be more suitable to represent the experimental beam profiles. Thus, transverse mode profiles $U_{mn}(r,z,\phi)$ were assumed to be described by Laguerre-Gaussian modes with different values of radial and azimuthal indices m and n in cylindrical coordinates [29,41]:

$$U_{mn}(r,z,\phi) = U^{LG}_{mn}(r,z)e^{in\phi}$$
$$U^{LG}_{mn}(r,z) = \frac{C^{LG}_{mn}}{w}\left(\frac{\sqrt{2}r}{w}\right)^{|n|} e^{-\frac{r^2}{w^2}} L^{|n|}_m\left(\frac{2r^2}{w^2}\right)\times e^{-ik\left(z+\frac{r^2}{2R(z)}\right)+i(2m+|n|+1)\psi(z)} \tag{10}$$

where C^{LG}_{mn} are the normalization constants calculated so that each mode intensity integrated over its transverse profile is equal to unity, L^n_m is the generalized Laguerre polynomial with radial and azimuthal indices m and n, $w = w_0\sqrt{1+(z/z_R)^2}$ and $R(z) = z(1+(z_R/z)^2)$ define the beam effective radius and radius of curvature of the phase front at distance z respectively, $\psi(z) = \arctan(z/z_R)$ is the Gouy phase shift, $z_R = \pi w_0^2/\lambda_e$ is the Rayleigh length, and w_0 is the waist radius of the fundamental mode. It can be estimated by the ideal cavity configuration as $w_0 = \sqrt{L\lambda/\pi}(1-L/R)^{1/4}$ and equals to 0.48 mm. In the ideal case of experimental configuration, the beam waist is located at the output mirror with a flat surface, while the averaged beam profiles were captured by the camera located at 41 cm from the output mirror. Thus, in the simulations, the LG modes are defined at $z = 0.4$ m to match the experimental conditions.

In the future analysis, it will be convenient to consider two degenerate LG modes with azimuthal indices $\pm n$ and transform these into two separate degenerate independent modes (cosine and sine):

$$\begin{aligned} U^{LG,cos}_{mn}(r,z,\phi) &= U^{LG}_{mn}(r,z)\cos(n\phi) \\ U^{LG,sin}_{mn}(r,z,\phi) &= U^{LG}_{mn}(r,z)\sin(n\phi) \end{aligned} \tag{11}$$

where $n > 0$ is now assumed. This basis is useful for representing the experimentally observed asymmetrical laser beam profiles as shown in Fig. 2b. Such beam profiles can appear for some anisotropic cavity configurations, where there is a dedicated spatial direction favorable for the generation of modes with a specific orientation (e.g. cosine-like), while the modes with another configuration are suppressed. In the simulations, we introduce this effect by different values of diffraction losses γ_{cos} and γ_{sin} for cosine and sine modes.

The maximal possible index of the lasing mode can be estimated from the Fresnel ratio and equals $F = 8$ for the aperture size in the cavity defined by the diameter of the Nd:YAG crystal (not limited by a diaphragm). In what follows, we consider 7 degenerate LG modes corresponding to 14 modes with cos- and sin-configurations taken as separate modes plus a fundamental Gaussian mode with $m = n = 0$. The mode set used in the simulations is shown in Fig. 2a. It was defined to match the most pronounced mode profiles observed in the experiments (Fig. 2b). Fig. 3 shows temporal profiles of the total and mode-dependent output Q-switched pulses obtained in the simulations for equal and different losses for cos- and sin-modes.

For an ideal plano-concave cavity configuration, when there are no mirror misalignments or other aberrations, the minimal frequency separation between transverse modes according to (2) is $\Delta\nu_t = 29.6$ MHz, which corresponds to the beating period $T_t = 1/\Delta\nu_t = 33.8$ ns. To obtain the rogue wave generation in experiments, a specific cavity configuration was required, which was obtained by adjusting the mirror positions (specifically, by introducing tilts in different directions). In this case, the cavity parameters g_1 and g_2 become different from the ones for the unperturbed cavity, which affects the mode frequencies

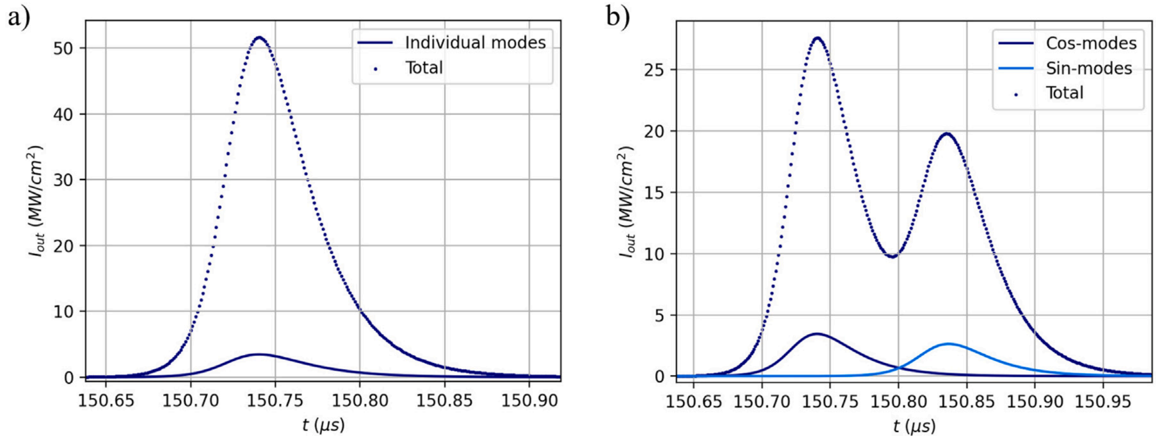

Fig. 3. Calculated temporal profiles of the output Q-switched pulses for (a) losses equal to 0.01 for all modes; (b) losses equal to 0.01 for cos-like modes and 0.04 for sin-like modes.

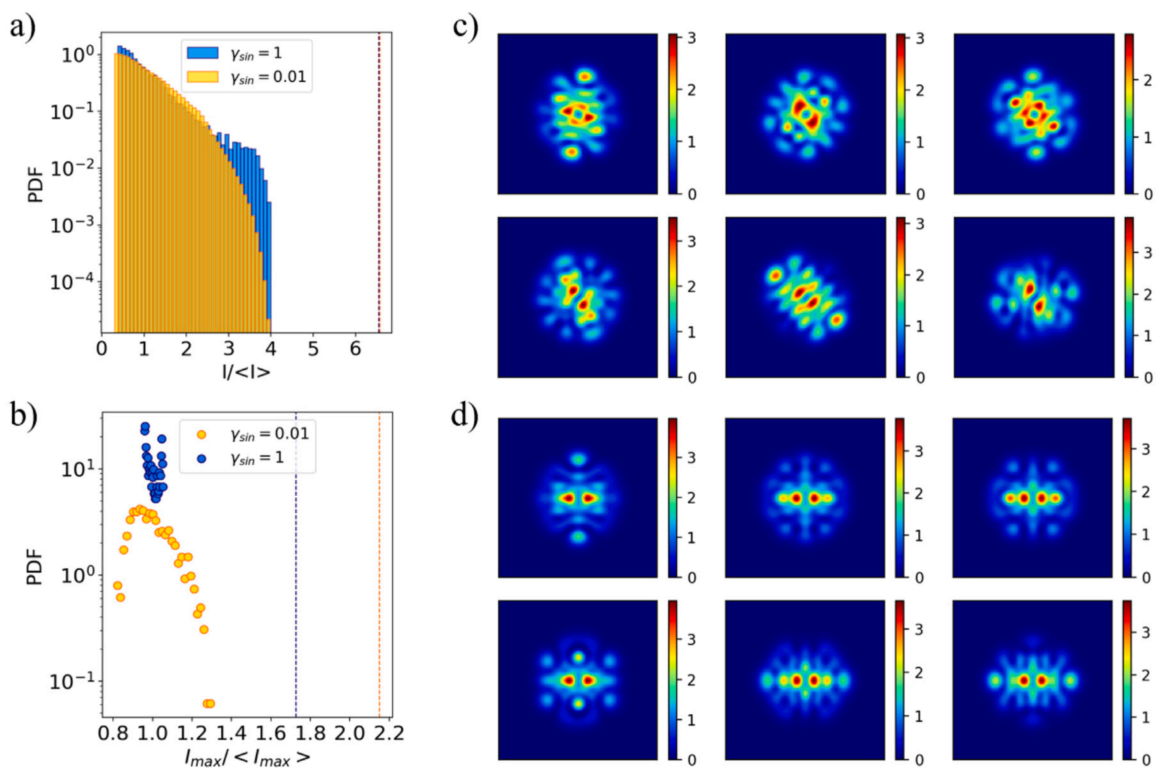

Fig. 4. Statistics of (a) intensity and (b) peak intensity over the beam profile for different values of losses in the cavity for modes with sine configuration; example output beam profiles (intensity relative to average) obtained in the simulation for (c) equal losses of 0.01 for all modes and (d) losses equal to 1 for modes with sine configuration (no spatial RWs are observed). Dashed lines indicate the rogue wave limits. The frequency separation between transverse modes is 29.6 MHz.

accordingly. To consider this effect in the simulations, we assume the frequency separation between transverse modes to be a free parameter that changes in the range from 0 to its maximal value of $c/(2L)$. This range of values is defined by the cavity stability conditions corresponding to $0 < g_1 g_2 < 1$. The frequencies of the transverse modes are then given by (1) for $q' = 2m + n + 1$.

The initial phases of the modes ϕ_{mn} are assumed to be randomly distributed in the range from 0 to 2π and uncorrelated for different modes and realizations of a Q-switched pulse.

3. Results

Our main result is that the frequency separation between transverse modes and anisotropy in the laser mode configuration represent two main factors that could affect the appearance of the rogue waves in our model and the corresponding experiments in [16]. To demonstrate this, we performed a number of simulations for different values of $\Delta\nu_t$ and losses for all modes with sine configuration γ_{sin}, while the losses for cosine-like modes γ_{cos} were set unchanged and equal to 0.01. For each of the input parameter sets, 1000 time-averaged intensity profiles $I_{average}(x, y)$ were obtained for different realizations of random initial phases of the transverse modes. We analyzed the rogue wave statistics in terms of two distributions. First is the distribution of intensity over all simulated beam profiles (2D distribution), which is characterized by the kurtosis parameter K. For fully developed speckle, the intensity statistics is described by a negative exponential distribution that has $K = 9$, while the statistics of real and imaginary parts are described by

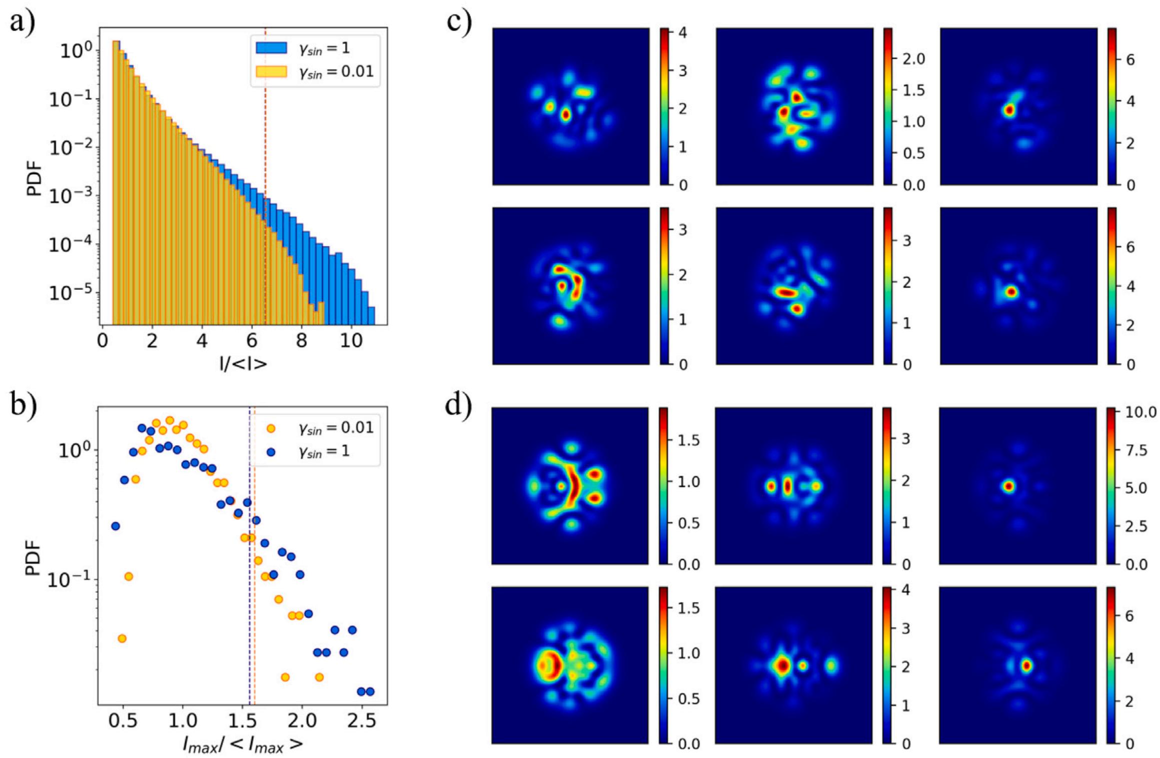

Fig. 5. Statistics of (a) intensity and (b) peak intensity over the beam profile for different values of losses in the cavity for modes with sine configuration; example output beam profiles (intensity relative to average) obtained in the simulation for (c) equal losses of 0.01 for all modes and (d) losses equal to 1 for modes with sine configuration (beam profiles with spatial RWs are shown in the rightmost columns). Dashed lines indicate the rogue wave limits. The frequency separation between transverse modes is 1 MHz.

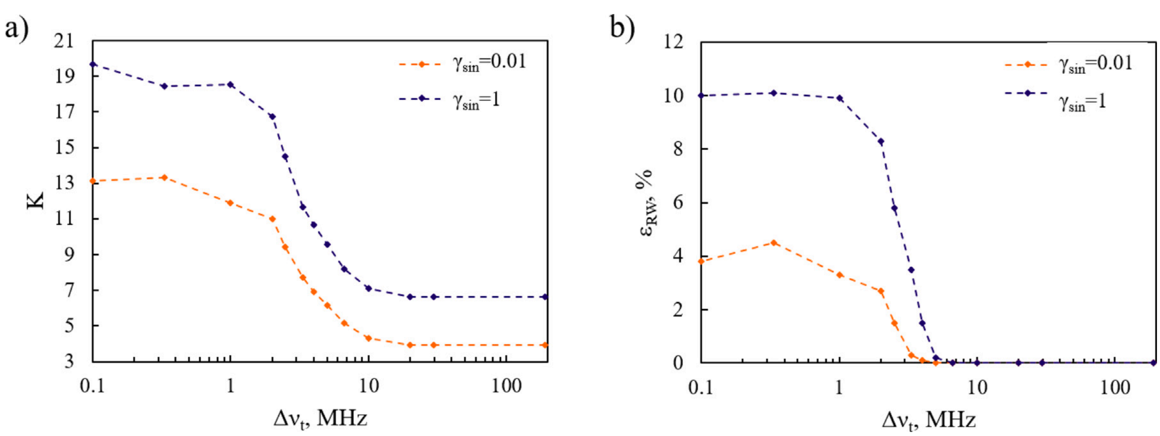

Fig. 6. Dependence of (a) kurtosis and (b) relative number of RWs on the frequency separation between transverse modes for different values of losses in the cavity for modes with sine configuration.

a normal distribution with $K = 3$ [43]. Thus, $K > 9$ characterizes an L-shaped intensity distribution deviating from the negative exponential one. Second is the distribution of peak intensities over the averaged beam profiles that gives information about the relative number of events corresponding to spatial RWs in the beam cross-section. The rogue wave limit was calculated from the 2D intensity distribution as $I_{RW} = (2A_{SWH})^2$, where A_{SWH} is the significant wave height for amplitudes. Background intensity values smaller than $0.1\langle I_{max}\rangle$ were discarded from the statistics.

Figs. 4–5 show the intensity statistics and random realizations of output beam profiles for two different values of frequency separation between the modes equal to 29.6 MHz and 1 MHz, respectively. Besides, Fig. 6 illustrates the dependence of kurtosis of the 2D intensity distribution and relative number of events containing RWs, ε_{RW} on the frequency separation between transverse modes $\Delta\nu_t$. Two limiting cases of laser mode configurations are considered here: the most isotropic case, which corresponds to $\gamma_{sin} = \gamma_{cos} = 0.01$ (losses are equal for all 15 modes), and the most anisotropic one, when $\gamma_{cos} = 0.01$ and $\gamma_{sin} = 1$ leading to negligible intensities of modes with sine configurations. From Fig. 6 one can see that in both cases the values of kurtosis and relative number of RWs increase with decreasing the frequency separation between modes (increasing the period of beating). Two representative values of $\Delta\nu_t$ in Figs. 4–5 correspond to two asymptotic values of kurtosis and ε_{RW} in Fig. 6. Fig. 4 illustrates an example of $\Delta\nu_t = 29.6$ MHz ($T_t = 33.8$ ns), which refers to an ideal cavity configuration. In this case the period of beating is small enough relatively to the Q-switched pulse duration (< 100 ns) and there are no spatial rogue waves in the output beam patterns as all beating effects between the modes are averaged out. Thus, the random beam patterns are similar to each other and do not exhibit strong intensity fluctuations. The opposite

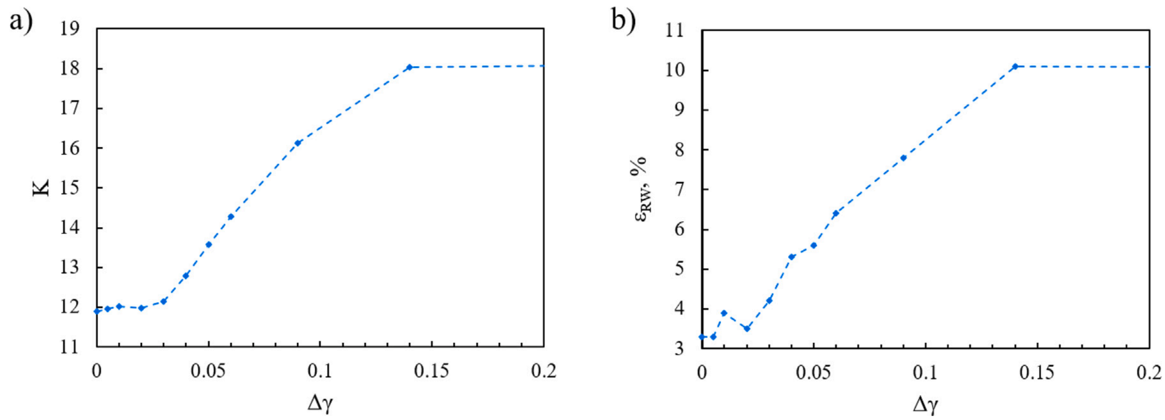

Fig. 7. Dependence of (a) kurtosis and (b) relative number of RWs on the difference of losses for sine and cosine modes. The frequency separation between transverse modes is 1 MHz.

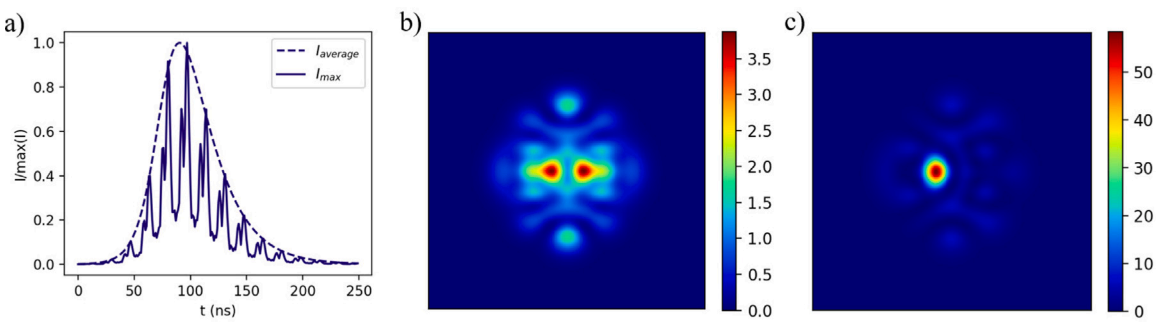

Fig. 8. (a) Temporal profiles of peak and spatially averaged intensity of the output beam normalized to their maximal values; (b) output beam profile averaged over the Q-switched pulse duration; (c) instantaneous output beam profile corresponding to maximal peak intensity (t = 97 ns). Output beam profiles in (b) and (c) are normalized to the value of <I> from Fig. 4a. The frequency separation between transverse modes is 29.6 MHz, and losses for sin-modes are equal to 1.

case is shown in Fig. 5 for ν_t = 1 MHz and the period of beating T_t = 1 μs, which is much larger than the Q-switched pulse duration. Under such conditions, the beating effects between the modes are not averaged out in the output beam profiles and random beam patterns vary significantly depending of the initial phases of the transverse modes. For specific values of initial phases ϕ_{mn}, spontaneous mode-locking occurs and an intense spatial rogue wave is formed as a result of constructive superposition of the modes with close locations of hot spots.

In addition, it can be seen from Fig. 6 that the values of kurtosis and relative number of RWs are about 1.5–2 times larger for γ_{sin} = 1 compared to γ_{sin} = 0.01. This indicates that anisotropic beam configurations are more favorable for spatial rogue waves formation in the time-averaged beam profiles.

The dependence of kurtosis and relative number of rogue wave events on the difference of losses in the cavity for sine and cosine modes is shown in Fig. 7. Both dependencies exhibit an almost linear growth till a limiting value of the loss difference $\Delta\gamma$ = 0.14, corresponding to negligible intensities of sin-modes compared to cos-modes. For increased losses for sin-modes, their corresponding Q-switched pulses have a reduced intensity and are generated later in time relative to Q-switched pulses for cos-modes, as demonstrated in an example in Fig. 3b. This leads to incoherent combinations of modes with different configurations and higher anisotropy in the output beam profiles, which is favorable for spatial RWs generation.

The results presented above were calculated for a specific case of output beam profiles averaged in time over the Q-switched pulse length. This allows for analyzing the formation of spatial rogue waves, but does not give any information about the temporal dynamics of rogue waves. To investigate this question, we calculated the time dependence of the peak intensity and spatially averaged intensity over the beam profile during the Q-switched pulse duration. Fig. 8a and Fig. 9a show examples of such dependencies for frequency spacing between the modes of 29.6 MHz and 1 MHz, respectively, and the most anisotropic mode configuration with only cos-modes involved in the laser generation (γ_{sin} = 1). The time-averaged output beam profiles and instantaneous beam profiles at the time moments corresponding to maximal peak intensity are shown in Fig. 8b,c and Fig. 9b,c. It is seen that in the case of small frequency separation between the modes (1 MHz in Fig. 9) the peak intensity and the spatially averaged intensity have very similar dependence on time, and the spatial structure of the output beam profile is almost unchanged during the Q-switched pulse generation. A spatial RW observed in the output beam profile has a lifetime close to the Q-switched pulse duration and a peak intensity almost 4 times higher than its time-averaged value. In contrast, the case of higher frequency separation between the modes presented in Fig. 8 indicates that the peak intensity over the beam profile can have specific time dynamics different from the one of the spatially-averaged intensity. It exhibits periodic behavior with several peaks and the period is equal to the period of beating between the modes (about 17 ns). Thus, the transverse beam profile is not stationary and changes considerably within the Q-switched pulse duration. A spatial rogue wave depicted in the instantaneous output beam profile (Fig. 8c) exists only during several ns and has the maximal intensity almost 15 times higher than the maximal intensity of the time-averaged beam profile, which does not contain any rogue waves. Thus, such spatial RW is actually a spatio-temporal rogue wave that emerges during the laser generation due to the spontaneous mode-locking effects but cannot be observed in the time-averaged beam profile captured by the camera. To detect and analyze these events experimentally, high-speed

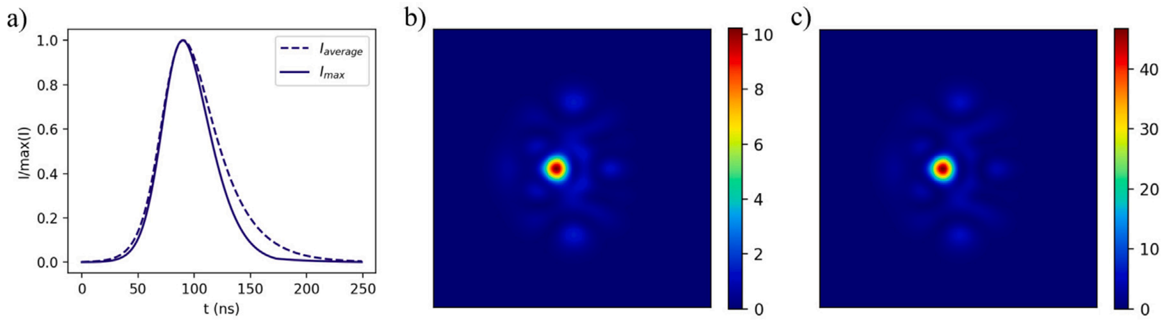

Fig. 9. (a) Temporal profiles of peak and spatially averaged intensity of the output beam normalized to their maximal values; (b) output beam profile averaged over the Q-switched pulse duration; (c) instantaneous output beam profile corresponding to maximal peak intensity (t=90 ns). Output beam profiles in (b) and (c) are normalized to the value of <I> from Fig. 5a. The frequency separation between transverse modes is 1 MHz, and losses for sin-modes are equal to 1.

photodetectors could be used along with special techniques such as spatial sampling and dispersive Fourier transformation, as described e.g. in [34].

4. Discussion

The theoretical model described in Section 2 is capable of reproducing spatial RWs generation in the time-averaged output laser beams with similar properties to those observed in the experiments as well as investigating the time dynamics of the transverse beam profiles. Specifically, the calculated values of kurtosis are close to the ones obtained in the experiments as well as the shape of 2D intensity PDFs. For frequency spacing between the modes less than several MHz, the calculated kurtosis values are larger than 9 indicating that 2D intensity distributions deviate from the negative exponential one and have a more pronounced L-shaped form.

Although the experimentally observed output beam profiles are not exactly reproduced by theoretical calculations, they exhibit similar peak intensities and hot spot sizes. The differences may be explained by non-exact representation of experimental mode profiles by LG modes as well as different losses for all modes, not only cos- and sin-like groups of modes. Besides, the maximal calculated probability of RWs generation is about 10% depending on the mode configuration, which is higher than observed experimentally (less than 1%). This may indicate that in experiments the frequency spacing between modes was relatively high leading to a smaller probability of RWs emergence. Also, only a subset of transverse modes could have been synchronized during the laser generation, while the other modes were interacting incoherently. This hypothesis or partial mode-locking is supported by experimental measurements of time dynamics and spatial coherence of the output laser beams, showing features characteristic of mode-locking effects [16]. Thus, coherent superposition of modes represents one of the mechanisms responsible for the spatial rogue wave generation in lasers. This observation is also supported by other studies, e.g. [15], where spatial RWs were generated for the case of partially developed speckle and caustic structures evolving from the coherent field with random phase.

Besides, the proposed theoretical model shows that in the case of a considerable frequency spacing between the modes the transverse beam profile can change dynamically and have a specific periodic time dependence of the peak intensity throughout the hot spots. The lifetimes of these hot spots can be in the order of several ns, which is much less than the entire Q-switched pulse duration. Such effect was also observed experimentally for beam profiles with well-developed speckle structure with and without spatial RWs [16]. However, the time resolution of the proposed theoretical model is limited by the cavity round-trip time (several ns). Besides, here we considered a simplified case of the transverse mode-locking assuming the laser generation at only one longitudinal mode. Simultaneous synchronization of both longitudinal and transverse modes could result in more complex temporal dynamics of the beam profile with periodic oscillations defined by the cavity round-trip time, which was indeed observed experimentally [16]. Thus, a more detailed analysis of the spatio-temporal mode-locking effects and RWs dynamics is left for future studies.

The last important observation refers to the dependence of RWs statistics on the mode configuration. Anisotropic mode configuration leads to a higher probability of RWs generation and higher values of kurtosis for intensity statistics than isotropic one. This effect was also noted in experimental studies [16]. In the laser setup, this can be obtained by introducing specific alignments of the cavity mirrors corresponding to different tilts and displacements in orthogonal axes. Thus, anisotropy of the mode configuration represents one of the symmetry-breaking mechanisms, which is favorable for spatial RWs emergence.

5. Conclusions

To conclude, we applied a simple theoretical model to simulate spatial and spatio-temporal rogue waves generation in an actively Q-switched solid-state laser with multiple transverse modes. Based on the modal representation of the total optical field in the cavity and rate equations for a point-like active medium, the model allows for simulating the mode-dependent Q-switched pulse generation neglecting the effect of nonlinear mode competition. Under such conditions, indicating the absence of nonlinear effects in the laser cavity, we show that spatial RWs can still be generated in the time-averaged output beam profiles depending on the values of certain laser parameters. One of such parameters is frequency spacing between transverse modes, which, if reduced, causes the transverse mode-locking leading to the formation of stationary hot spots in the output beam profiles. In the case of higher values of the frequency spacing, the spatial beam distribution exhibits oscillating time dynamics with the tendency to form transient spatio-temporal rogue waves. Another important parameter is the anisotropy of the mode configuration, which leads to spatial symmetry breaking in the system and considerably increases the probability of RWs generation. Such observations suggest that transverse mode locking and spatial anisotropy of the mode configuration represent factors leading to RWs formation in multimode lasers even with negligible nonlinear effects.

CRediT authorship contribution statement

Roza Navitskaya: Conceptualization, Investigation, Methodology, Visualization, Software. **Ihar Stashkevich:** Conceptualization, Investigation, Resources, Supervision. **Stanislav Derevyanko:** Conceptualization, Investigation, Resources, Supervision. **Alina Karabchevsky:** Conceptualization, Funding acquisition, Investigation, Supervision.

Declaration of competing interest

The authors declare that they have no known competing financial interests or personal relationships that could have appeared to influence the work reported in this paper.

Data availability

Data will be made available on request.

Acknowledgment

The research was funded by Israel Science Foundation ISF no. 2598/20.

References

[1] D.R. Solli, C. Ropers, P. Koonath, B. Jalali, Optical rogue waves, Nature 450 (2007) 1054.
[2] N. Akhmediev, et al., Roadmap on optical rogue waves and extreme events, J. Opt. 18 (2016) 063001.
[3] Y. Song, Z. Wang, K.P. Cong Wang, H. Zhang, Recent progress on optical rogue waves in fiber lasers: status, challenges, and perspectives, Adv. Photonics 2 (2020) 024001.
[4] J.M. Dudley, G. Genty, A. Mussot, A. Chabchoub, F. Dias, Rogue waves and analogies in optics and oceanography, Nat. Rev. Phys. 1 (2019) 675–689.
[5] C. Bonazzola, A. Hnilo, M. Kovalsky, J. Tredicce, Extreme events and single-pulse spatial patterns observed in a self-pulsing all-solid-state laser, Phys. Rev. E 97 (2018) 032215.
[6] G. Arisholm, Self-focusing and optical damage in a diode-pumped neodymium laser, in: OSA TOPS, Vol. 10, in: Advanced Solid State Lasers, 1997, p. 109, (Optical Soc. Am., 1997).
[7] P.M. Lushnikov, N. Vladimirova, Non-gaussian statistics of multiple filamentation, Opt. Lett. 35 (2010) 12.
[8] H. Qin, X. Xiao, P. Wang, C. Yang, Observation of soliton molecules in a spatiotemporal mode-locked multimode fiber laser, Opt. Lett. 43 (2018) 9.
[9] Y. Ding, X. Xiao, P. Wang, C. Yang, Multiple-soliton in spatiotemporal mode-locked multimode fiber lasers, Opt. Express 27 (2019) 8.
[10] C. Rimoldi, S. Barland, F. Prati, G. Tissoni, Spatiotemporal extreme events in a laser with a saturable absorber, Phys. Rev. A 95 (2017) 023841.
[11] K. Talouneh, C. Rimoldi, R. Kheradmand, G. Tissoni, M. Eslami, Control of spatiotemporal rogue waves by harmonic pump modulation in a semiconductor laser with a saturable absorber, Phys. Rev. A 102 (2020) 033508.
[12] C. Liu, R.E.C. van der Wel, N. Rotenberg, L. Kuipers, T.F. Krauss, A.D. Falco, A. Fratalocchi, Triggering extreme events at the nanoscale in photonic seas, Nat. Phys. 11 (2015) 358–363.
[13] F. Arecchi, U. Bortolozzo, A. Montina, S. Residori, Granularity and inhomogeneity are the joint generators of optical rogue waves, Phys. Rev. Lett. 106 (2011) 153901.
[14] C. Bonatto, S.D. Prado, F.L. Metz, J.R. Schoffen, R.R.B. Correia, J.M. Hickmann, Super rogue wave generation in the linear regime, Phys. Rev. E 102 (2020) 052219.
[15] A. Mathis, L. Froehly, S. Toenger, F. Dias, G. Genty, J.M. Dudley, Caustics and rogue waves in an optical sea, Sci. Rep. (2015) 12822.
[16] R. Navitskaya, I. Stashkevich, S. Derevyanko, A. Karabchevsky, Spatial rogue waves in the actively Q-switched nd:YAG laser under low Kerr nonlinearity, Opt. Express 30 (2022) 37076–37084.
[17] D.H. Auston, Transverse mode locking, IEEE J. Quantum Electron. 4 (1968) 420–422.
[18] P.W. Smith, Mode-locking of lasers, Proc. IEEE 58 (1970) 1342–1357.
[19] C. Haug, F.W. Dabby, Transverse mode locking using cylindrically symmetric modes, IEEE J. Quantum Electron. 7 (1971) 489–491.
[20] F. Schepers, T. Hellwig, C. Fallnich, Modal reconstruction of transverse mode–locked laser beams, Appl. Phys. B 126 (2020) 168.
[21] P.W. Smith, Simultaneous phase-locking of longitudinal and transverse laser modes, Appl. Phys. Lett. 13 (1968) 235–237.
[22] V.S. Arakelyan, N.V. Karlov, A.M. Prokhorov, Self synchronization of transverse modes of a CO_2 laser, JETP Lett. 10 (1969) 178–180.
[23] M. Michon, J. Ernest, R. Auffret, Passive transverse mode locking in a confocal Nd3+ glass laser, IEEE J. Quantum Electron. 5 (1969) 125–126.
[24] M. Kowalczyk, T. Martynkien, P. Mergo, G. Sobon, J. Sotor, Ultrabroadband wavelength-swept source based on total mode-locking of an Yb:CaF2 laser, Photonics Res. 7 (2019) 182–186.
[25] D. Cote, H.M. van Driel, Period doubling of a femtosecond Ti:sapphire laser by total mode locking, Opt. Lett. 23 (1998) 715–717.
[26] S.R. Bolton, R.A. Jenks, C.N. Elkinton, G. Sucha, Pulse-resolved measurements of subharmonic oscillations in a Kerr-lens mode-locked Ti:sapphire laser, J. Opt. Soc. 16 (1999) 339–344.
[27] J.H. Lin, M.D. Wei, W.F. Hsieh, H.H. Wu, Cavity configurations for soft-aperture Kerr-lens mode-locking and multiple period bifurcations in Ti:sapphire lasers, J. Opt. Soc. Amer. B 18 (2001) 1069–1075.
[28] H.H. Wu, C.R. Huang, J.T. Huang, Spatiotemporal dynamics of a passively mode-locked Nd:GdVO4 laser, Opt. Express 15 (2007) 2391–2397.
[29] Z. Zhang, C. Zhao, Spontaneous phase and frequency locking of transverse modes in different orders, Phys. Rev. A 13 (2020) 024010.
[30] R. Gordon, A.P. Heberle, J.R.A. Cleaver, Transverse mode-locking in microcavity lasers, Appl. Phys. Lett. 81 (2002) 4523–4525.
[31] B. Zhang, D.W. Snoke, A.P. Heberle, Towards the transverse mode-locking of oxide-confined VCSELs, Opt. Commun. 285 (2012) 4117–4119.
[32] Y. Sun, S. Combrie, F. Bretenaker, A.D. Rossi, Mode locking of the Hermite-Gaussian modes of a nanolaser, Phys. Rev. Lett. 123 (2019) 233901.
[33] L.G. Wright, D.N. Christodoulides, F.W. Wise, Spatio-temporal mode-locking in multimode fiber lasers, Science 358 (2017) 94–97.
[34] K. Liu, X. Xiao, Y. Ding, H. Peng, D. Lv, C. Yang, Buildup dynamics of multiple solitons in spatiotemporal mode-locked fiber lasers, Photonics Res. 9 (2021) 1898–1906.
[35] G. D'Alessandro, F. Papoff, E. Louvergneaux, P. Glorieux, Average patterns and coherent phenomena in wide aperture lasers, Phys. Rev. E 69 (2004) 066212.
[36] F. Encinas-Sanz, S. Melle, O.G. Calderon, Time-resolved dynamics of two-dimensional transverse patterns in broad area lasers, Phys. Rev. Lett. 93 (2004) 213904.
[37] E. Cabrera, S. Melle, O.G. Calderon, J.M. Guerra, Dynamic transition from modelike patterns to turbulentlike patterns in a broad-area Nd:YAG laser, Opt. Lett. 31 (2006) 1067–1069.
[38] K. Staliunas, M.F.H. Tarroja, C.O. Weiss, Transverse mode locking, antilocking and self-induced dynamics of class-B lasers, Opt. Commun. 102 (1993) 69–75.
[39] K.W. Ho, J.W. Liang, T.W. Lin, C.P. Chiu, C.H. Chen, M.D. Wei, Spontaneous chaos and extreme events in a solid-state laser with the transverse-mode-degenerate cavity configuration, Opt. Lett. 48 (2023) 1308–1311.
[40] T. Mayteevarunyoo, B.A. Malomed, D.V. Skryabin, Spatiotemporal dissipative solitons and vortices in a multi-transverse-mode fiber laser, Opt. Express 27 (2019) 37364.
[41] H. Kogelnik, T. Li, Laser beams and resonators, Appl. Opt. 5 (1966) 1550–1567.
[42] O. Svelto, Principles of Lasers, fifth ed., Springer, 2010.
[43] J.W. Goodman, Speckle Phenomena in Optics: Theory and Applications, SPIE, 2020.